AFRL-AFOSR-JP-TR-2022-0006

Advanced methods to substantially achieve the multi-functional infrared sensors technologies for multi-spectral and polarimetric infrared images

Lee, Sang Jun
KOREA RESEARCH INSTITUTE OF STANDARDS AND SCIENCE (KRISS)
1 DORYONG DONG YUSEONG GU
DAEJUN-CITY, ,
KR

11/29/2021
Final Technical Report

Air Force Research Laboratory
Air Force Office of Scientific Research
Asian Office of Aerospace Research and Development
Unit 45002, APO AP 96338-5002

REPORT DOCUMENTATION PAGE

Form Approved
OMB No. 0704-0188

1. REPORT DATE *(DD-MM-YYYY)*	**2. REPORT TYPE**	**3. DATES COVERED** *(From - To)*
29-11-2021	Final	23 Aug 2018 - 22 Aug 2021

4. TITLE AND SUBTITLE
Advanced methods to substantially achieve the multi-functional infrared sensors technologies for multi-spectral and polarimetric infrared images

5a. CONTRACT NUMBER
FA2386-18-1-4021

5b. GRANT NUMBER

5c. PROGRAM ELEMENT NUMBER
61102F

6. AUTHOR(S)
Sang Jun Lee

5d. PROJECT NUMBER

5e. TASK NUMBER

5f. WORK UNIT NUMBER

7. PERFORMING ORGANIZATION NAME(S) AND ADDRESS(ES)
KOREA RESEARCH INSTITUTE OF STANDARDS AND SCIENCE (KRISS)
1 DORYONG DONG YUSEONG GU
DAEJUN-CITY,
KR

8. PERFORMING ORGANIZATION REPORT NUMBER

9. SPONSORING/MONITORING AGENCY NAME(S) AND ADDRESS(ES)
AOARD
UNIT 45002
APO AP 96338-5002

10. SPONSOR/MONITOR'S ACRONYM(S)
AFRL/AFOSR IOA

11. SPONSOR/MONITOR'S REPORT NUMBER(S)
AFRL-AFOSR-JP-TR-2022-0006

12. DISTRIBUTION/AVAILABILITY STATEMENT
A Distribution Unlimited: PB Public Release

13. SUPPLEMENTARY NOTES

14. ABSTRACT
We have designed, fabricated and characterized surface plasmonic structures for multispectral and polarization imaging sensors. We introduced two periodic array structures of square coaxial aperture (SCA) and quasi-three-dimensional circular coaxial aperture (quasi-3D CCA) onto InAs/GaSb type-II superlattice (T2SL) photodetectors. By adjusting the pitch of the array, multispectral filtering of the SCA and quasi-3D CCA integrated T2SL detectors is successfully performed at the detector level in the spectral ranges of 2.4–4 μm and 3–5 μm, respectively. In addition, we have developed a fabrication process for large-area (2×2) super pixelated subwavelength gold gratings with four different orientations of 0°, 45°, 90°, and 135°, using UV nanoimprint lithography. This process can be adopted as a promising technique to fabricate next-generation large-format polarimetric imagers with high extinction ratio.

15. SUBJECT TERMS

16. SECURITY CLASSIFICATION OF:			**17. LIMITATION OF ABSTRACT**	**18. NUMBER OF PAGES**	**19a. NAME OF RESPONSIBLE PERSON**
a. REPORT	**b. ABSTRACT**	**c. THIS PAGE**			TONY KIM
U	U	U	SAR	11	**19b. TELEPHONE NUMBER** *(Include area code)* 315-227-7008

Final Performance Report

PROJECT TITLE: **Metamaterial based pixel-level infrared imager for adaptive sensing**

AWARD NO: **FA2386-18-1-4021**

PRINCIPAL INVESTIGATOR:

Dr. Sang Jun Lee, Principal Research Scientist

Korea Research Institute Standards and Science

Email: sjlee@kriss.re.kr, Phone: +82 42 868 5127, Fax: +82 42 868 5047

Address: 267 Gajeong-ro, Yuseong-gu, Daejeon 34113, Korea

I. Accomplishments

Journal paper

- J. Jeon, J. Hwang, V. M. More, D.-K. Kim, Y. Kim and S. J. Lee, "Wavelength Tuning of Type-II Superlattice Spectral Response Using a Square Coaxial Aperture Array," ***Journal of Lightwave Technology*** 39, 4684 (2021).

II. Technical Progress

Wavelength tuning of type-II superlattice spectral response using a square coaxial aperture array

Infrared spectral imaging systems are typically implemented by combining a traditional camera system with optical components, but these systems are extremely bulky, have complex alignment, high cost, and cannot perform scanning in real-time. To address these drawbacks, infrared sensors integrated with multicolor functionality are being developed. Numerous studies have explored infrared sensors by combining them with plasmonic metamaterials, micro Fabry-Perot filters as elements with multicolor capability. We propose a square coaxial aperture (SCA) array structure for multi-spectral sensing (**Figure 1a**). The metal hole array (MHA) based plasmonic structure have been widely investigated for wavelength selection due to their surface plasmon resonance. However, as you see the **Figure 1b**, the MHA cannot achieve transmittance at one specific wavelength due to the harmonics generated by surface plasmon resonance. In

addition, the resonance peak depends on the angle of the incident light, thereby rendering MHA unsuitable for wavelength tuning. On the contrary, the SCA has Gaussian shaped-peak resonance with high transmission. Unlike the MHA structure, a square metal disk with w_1 on one side is formed at the center of the SCA. The square metal disk in the coaxial aperture promotes enhanced transmission, which is shown by the waveguide resonance effect. The waveguide resonance corresponds to the coupling of electric field to the TE_{10} mode in the gap (between the inner and the external width metallic surfaces, i.e., waveguide cavity).

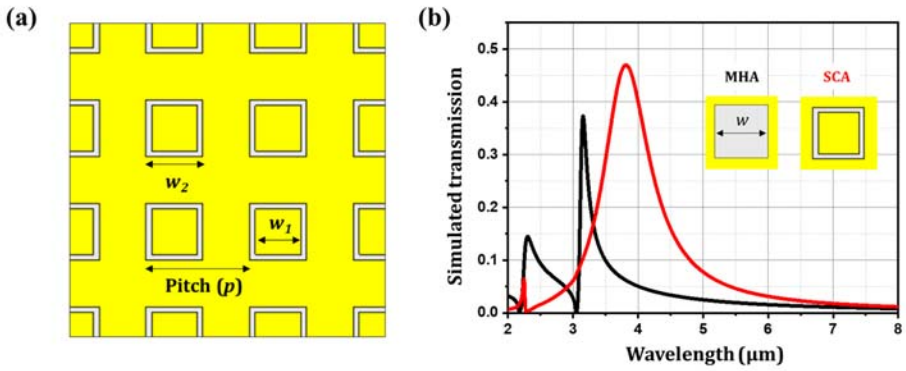

Figure 1 | (a) Schematic of the square coaxial aperture array (SCA) on the GaSb substrate. The pitch, inner, and external width and gap of the SCA are labeled as p, w_1 and w_2, respectively. (b) The transmission spectra of metal hole array (MHA) (black solid line) and SCA (red solid line) at p = 0.8 μm, $w = w_2$ and w_1 is 0.44 μm and 0.352 μm, respectively. Inset is the schematic view of the two structures to compare the transmissions.

To investigate the structural properties of the SCA structure, we performed a finite-difference time-domain (FDTD) based simulation (CST Microwave studio). As you can see the **Figure 2**, the transmission of the structure changes according to the w_2, w_1, p and incident angle of light. As w_2 increases (**Figure 2a**), the opening area becomes wider and the transmission increases. However, as the full width at half maximum (FWHM) increases, it cannot function as a filter having a peak at a specific wavelength. On the other hand, when w_1 is decrease (**Figure 2b**), it changes to the shape of MHA and other peaks due to harmonics. If w_1 and w_2, having Gaussian type transmission are fixed and the pitch is changed (**Figure 2c**), the peak appears at a longer wavelength as the pitch increases. Finally, it was confirmed that the shape of the transmission did not change according to the angle of the incident light (**Figure 2d**).

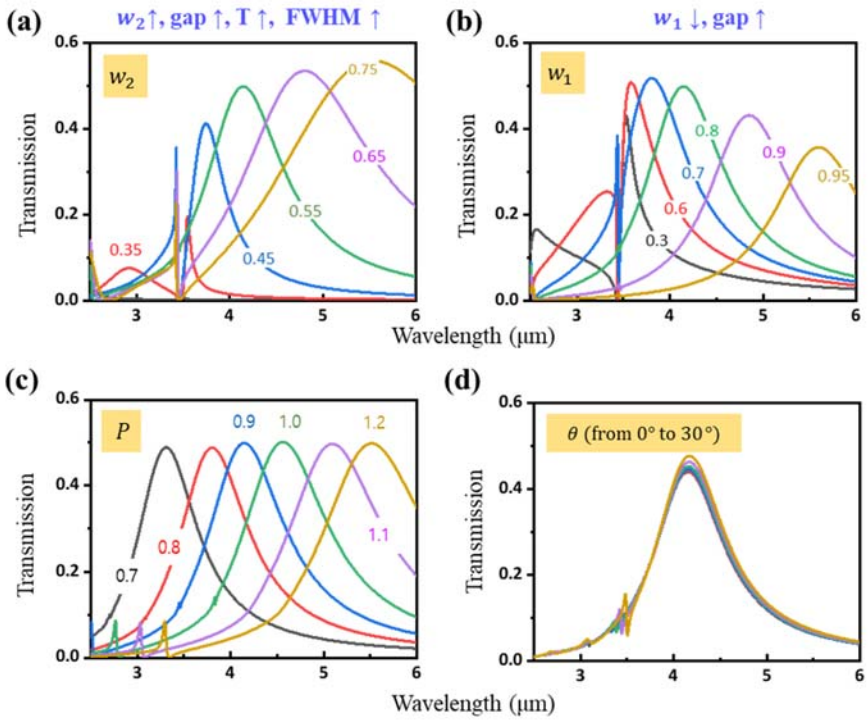

Figure 2 | Simulated transmission spectra according to (a) w_2, (b) w_1, (c) p and (d) incident angle of light.

Based on these observations, we set the parameter of the SCA before creating a pattern on the InAs/GaSb type-II superlattice (T2SL) single-pixel device. The device was fabricated via mesa formation, surface passivation, and ohmic metal deposition. First, an array mesa of 410 μm × 410 μm size was formed using standard photolithography and dry-etched using an inductively coupled plasma (ICP) by BCl_3 gas. To reduce the damage from dry etching, wet etching was performed using a mixed solution of H_3PO_4 : H_2O_2 : H_2O = 1 : 2 : 20. Next, a 200 nm of SiO_2 was deposited using plasma enhanced chemical vapor deposition for surface passivation. Finally, when the ohmic contact metal of Ti/Pt/Au (50/50/250 nm) was deposited by an electron beam evaporator, a single pixel with a window of 300 μm was formed. To verify the response of the fabricated device, the Nicolet 5700 Fourier transform infrared spectrometer (FTIR) with a KEITHLEY model 428 current amplifiers was used. Each SCA was fabricated on the window of the single pixel (SEM image shown in **Figure 3a**) using electron beam lithography (EBL); this caused the structure to have different geometrical parameters. The **Figure 3b** depicts a comparison the experimental values with those of the simulation of w_1, w_2 and ρ ($\rho = (w_2^2 - w_1^2)/p^2$, opening area ratio). The values of w_1 and w_2 are seen to differ slightly. For ρ, the designed structure had a uniform rate of

10.9% because f_1 and f_2 are fixed. However, the experimental value represents an average of 20% over the simulated value as w_1 decreases and w_2 increases. This can be attributed to the imperfections and variations that generally occur during the fabrication process.

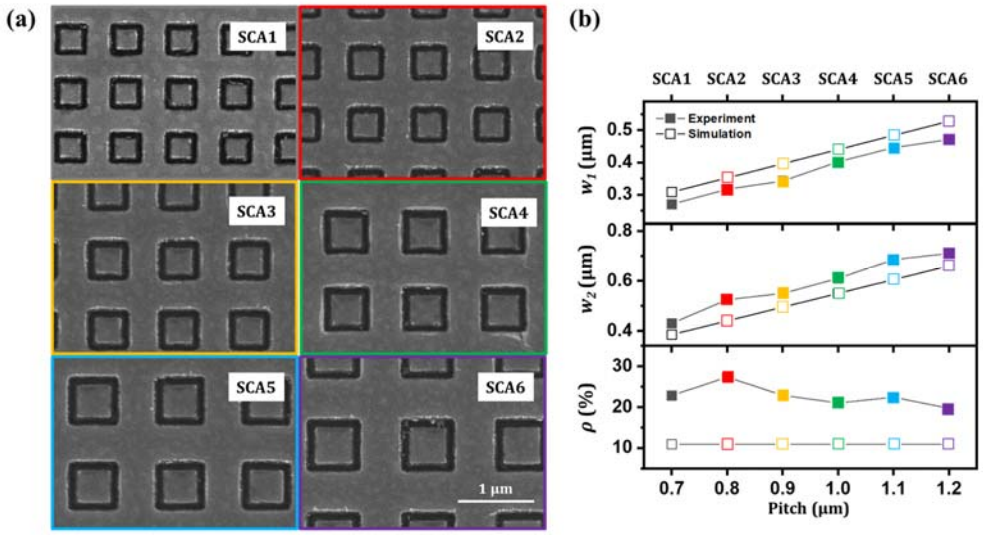

Figure 3 | (a) SEM images of the fabricated SCA structures using electron beam lithography (note: the scale bar of all SEM images is 1 μm) on the window of single pixel. (b) Comparison between the experimental and the simulated values of w_1, w_2, and ρ.

The device simulations were conducted to predict the peak wavelength of measured spectral responsivity using FDTD simulation. Responsivity measurements were performed by applying radiation from a Mikron M360 blackbody, calibrated at T = 900 K, onto the SCA-T2SL single-pixel. The blackbody radiation was modulated at a frequency of 400 Hz using a chopper, and the signal from the chopper was used as a trigger for the SRS 770 fast Fourier transforms network analyzer from the Stanford Research Systems. The single-pixel devices without/with the SCA and are called the bare-T2SL and SCA-T2SL. **Figure 4a** shows the measured spectral responsivity of the bare-T2SL device (blue solid line, right y-axis) and the fabricated SCA-T2SL (red solid line, right y-axis) device with an applied bias of –300 mV at 77 K. As mentioned earlier, the FWHM of the measured SCA-T2SL widened. Moreover, the responsivity peak at 2.75 μm was influenced by the responsivity of bare-T2SL. Also, black dashed line presents the value of simulated spectral response (left y-axis) of the device. **Figure 4b** displays the peak wavelengths of the measured spectral responsivity of SCA-T2SL (red line); the values from SCA1 to SCA6 are

2.35, 2.71, 3.249, 3.57, 3.86 and 4.1 μm, respectively, which verifies the wavelength tuning of the bare-T2SL (λ = 4.59 μm, black line) device. Additionally, the corresponding peak wavelengths of SCA-T2SL according to the simulation results are 2.37, 2.77, 3.13, 3.44, 3.93 and 4.14 μm. Futhermore, the dark current of Bare-T2SL device is comparable with that of SCA-T2SL devices, as shown in **Figure 4c**. This indicates that no degradation in the dark current is present after integrating the SCA arrays onto Bare-T2SL device.

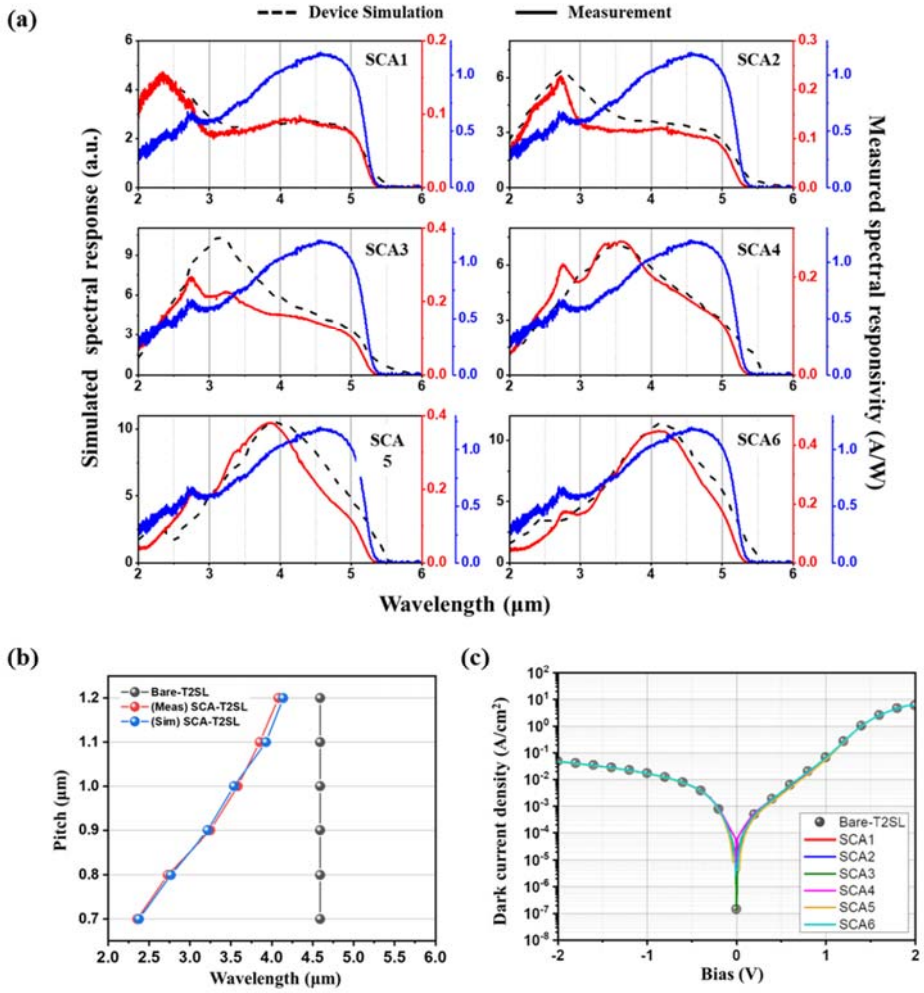

Figure 4 | (a) Simulated spectral response and measured spectral responsivity. The spectral responsivity of SCA-T2SLs (red solid line, right y-axis) and bare-T2SL (blue solid line, right y-axis) applied bias of – 300 mV at 77 K. (b) Peak wavelength of the measured Bare- and SCA-T2SL, and device simulated SCA-T2SL. The plot clearly shows the peak wavelength tuning. (c) Dark current density-voltage characteristics of Bare-T2SL and SCA-T2SL device measured at 77 K.

Design, fabrication and characterization of quasi-three-dimensional coaxial aperture arrays

The fabrication process of a quasi-three-dimensional coaxial aperture array (quasi-3D CCA) structure is illustrated in **Figure 5**. A 500 nm-thick benzocyclobutene (BCB) polymer is spin-coated on a 2-inch GaAs substrate at 5000 rpm for 30 s and cured on a hot plate at 250°C for 1 hr (Step 2). In the scanning electron microscopy (SEM) image, the BCB layer has a uniform flat surface and a clear interface between the coating and substrate. AZ5206 photoresist is spun on the BCB layer at 5000 rpm for 30 s and patterned using photolithographic techniques (Step 3). Then, the BCB layer is etched to precisely adjust the gap of the coaxial aperture using a reactive ion etcher (RIE) with O_2/CF_4 (50 sccm/10 sccm) plasma gases (Step 4). During the RIE process, the patterned photoresist serves as an etch mask with high etch selectivity. The remaining photoresist is completely removed in acetone and then a 50 nm-thick Au layer is deposited on the front surface by electron beam evaporation (Step 6). Fabricated quasi-3D CCA structrures have varying geometrical parameters of the pitch ranging from p = 1.8 μm to 3.2 μm with a step of 0.2 μm and the gap width of w_{gap} = 100, 180, and 270 nm.

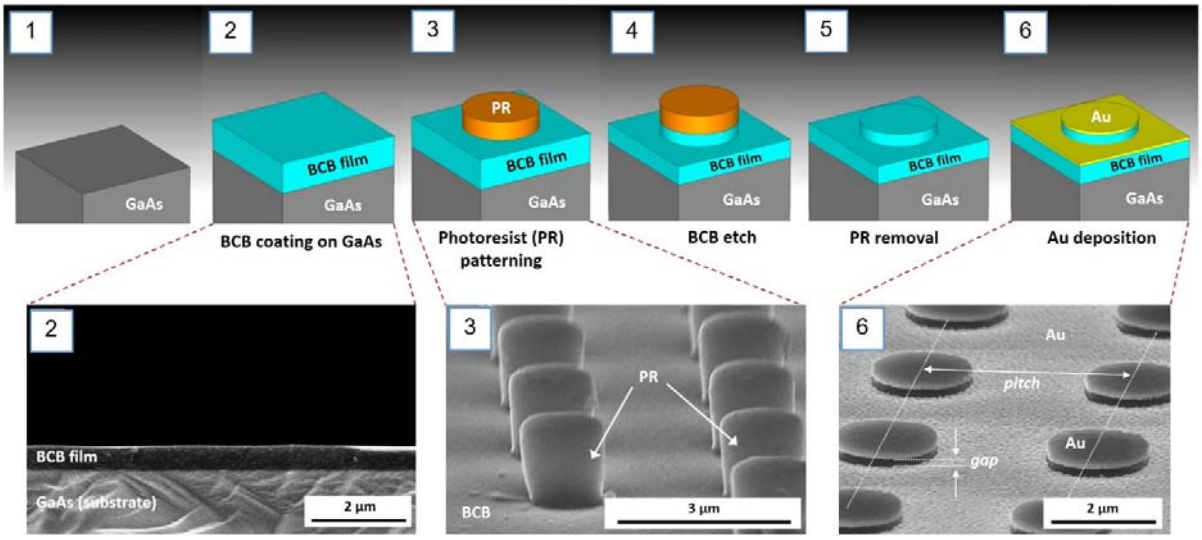

Figure 5 | Schematic of the fabrication process flow for the quasi-three-dimensional coaxial aperture array (quasi-3D CCA) and the measured SEM image indicating the geometrical parameters of the pitch (p) and gap width (w_{gap}).

Figure 6a shows the measured transmission spectra of the quasi-3D CCA structures with a fixed gap width of w_{gap} = 180 nm and different pitches ranging from p = 1.8 μm to 3.2 μm with a step of 0.2 μm. It is clear that the transmission peak is shifted toward longer wavelengths as the pitch increases. The measured and simulated results for the relationship between the transmission peak and the pitch have good agreement with each other (**Figure 6b**). This transmission peak redshift is attributed to the mode coupling of the first order surface plasmon at the Au hole/BCB interface and the localized surface plasmon of the Au disk array. **Figures 6c-e** exhibit the measured transmission spectra of the CCA structures with a fixed pitch and different gap widths of w_{gap} = 100, 180, and 270 nm. As the gap width increases the transmission peak is shifted toward shorter wavelengths. The reduction of the gap width enhances the electrostatic and radiative fields at the edges of the Au hole and disk array, leading to the increase in the surface polarization. As a result, the restoring force for the coherent electron oscillation on the disk surface is reduced, giving rise to the reduction of an effective spring constant (k_{eff}). Thus, the transmission peak (λ_p) is blueshifted with increasing the gap width ($\lambda_p \propto 1/\sqrt{k_{eff}}$).

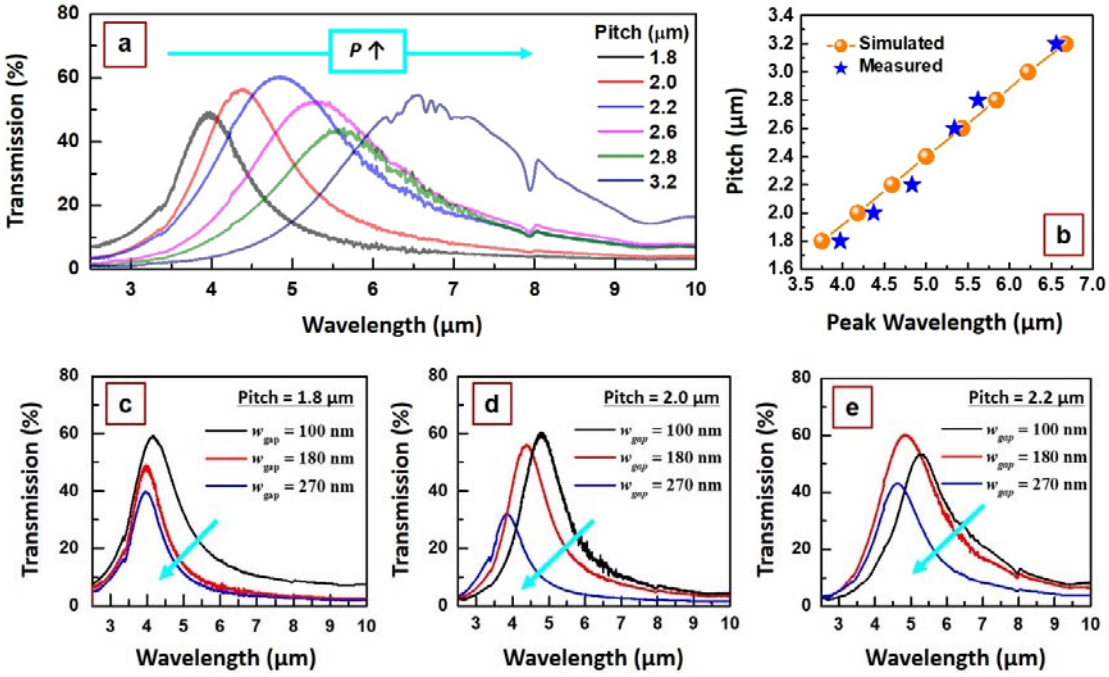

Figure 6 | (a) Measured transmission spectra of quasi-3D CCA structures with varying the pitch, (b) peak wavelength *vs* pitch, measured transmission spectra with different gap widths (w_{gap}) at a fixed pitch of (c) 1.8 μm, (d) 2.0 μm, and (e) 2.2 μm.

Fabrication and characterization of a multispectral photodetector integrated with a quasi-three-dimensional coaxial aperture array

The fabrication of a multispectral photodetector integrated with a quasi-three-dimensional coaxial aperture array is schematically illustrated in **Figure 7**. A 1 μm-thick SU-8 resist is spin-coated on a T2SL/silicon fanout chip at 4000 rpm for 30 s and cured on a hot plate at 150°C for 30 min (Step 2). A polydimethylglutarimide (PMGI) resist is spun on the SU-8 layer, followed by spin-coating of a ultraviolet (UV) curable LV400 resist on the PMGI resist (Step 3). UV nanoimprint lithography (NIL) is used to transfer the array patterns onto the LV400 resist. After NIL imprinting, the residual LV400 and PMGI resists are etched by reactive ion etching (RIE) using a mixture of CF_4 and O_2 plasma gases (Step 4). A 10 nm-thick Cr layer is deposited on the sample by electron beam evaporation at low deposition rate and then a lift-off process is conducted (Step 5). The SU-8 layer is etched by a gap width of w_{gap} = 100 nm by a RIE process to form SU-8 nanopost (Step 6). Finally, a 50 nm-thick Au layer is deposited on the front surface by electron beam evaporation (Step 7).

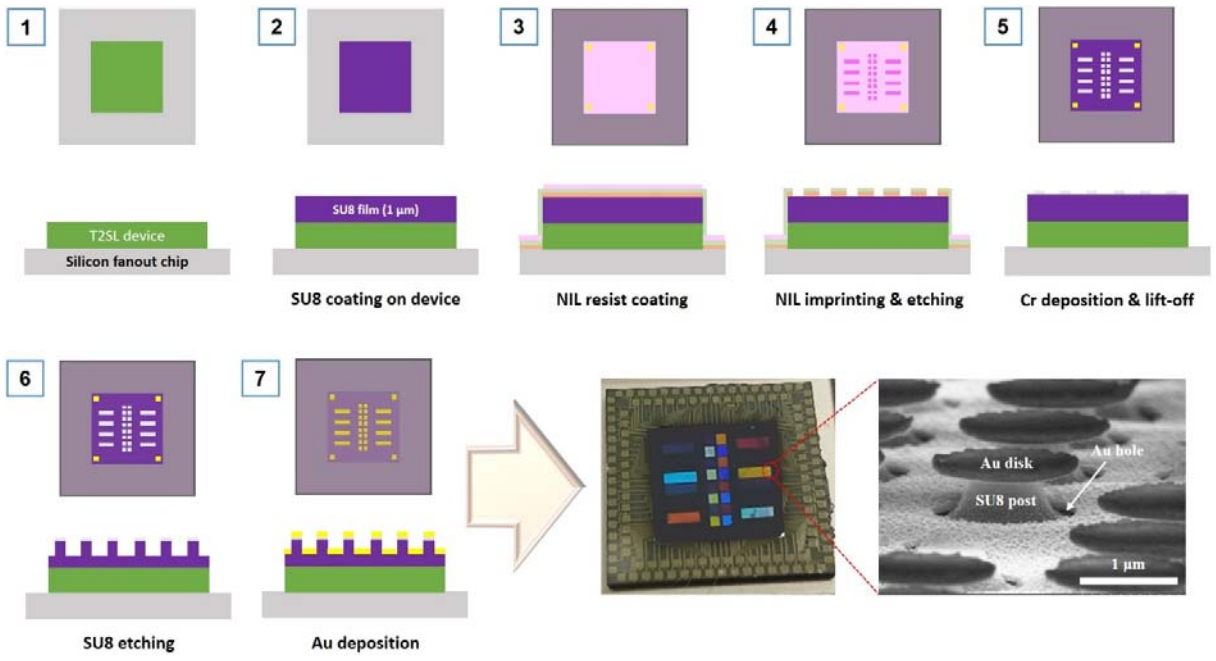

Figure 7 | Schematic of the fabrication process flow for the multispectral photodetector integrated with a quasi-three-dimensional coaxial aperture array.

Figure 8a shows the spectral response of the as-fabricated type-II superlattice (T2SL) photodetector measured by a Fourier transform infrared spectrometer at 77 K. The absorber of the T2SL photodetector consists of 300 periods of InAs(10 ML)/GaSb(10 ML)/InSb (1 ML) layers, leading to an effective energy band gap of ~0.22 eV at 77 K. The 90% cutoff wavelength is measured to be ~5.6 μm, as seen in the spectral response. **Figure 8b** represents the measured spectral responses of the T2SL photodetector integrated with a quasi-three-dimensional coaxial aperture array (quasi-3D CCA) with different pitches. As the pitch increases from p = 1.2 μm to 2.0 μm, the main peak is redshifted from 3.75 μm to 5.25 μm due to mode coupling of the surface plasmons of the Au hole and disk array. This clearly demonstrates the multispectral filtering in the mid-wavelength infrared band (3–5 μm) at on-chip level. In addition, the quasi-3D CCA structure can be applied as a plasmonic spectral filter to an infrared focal plane array sensor for multispectral imaging, which provides higher spectral and spatial resolution.

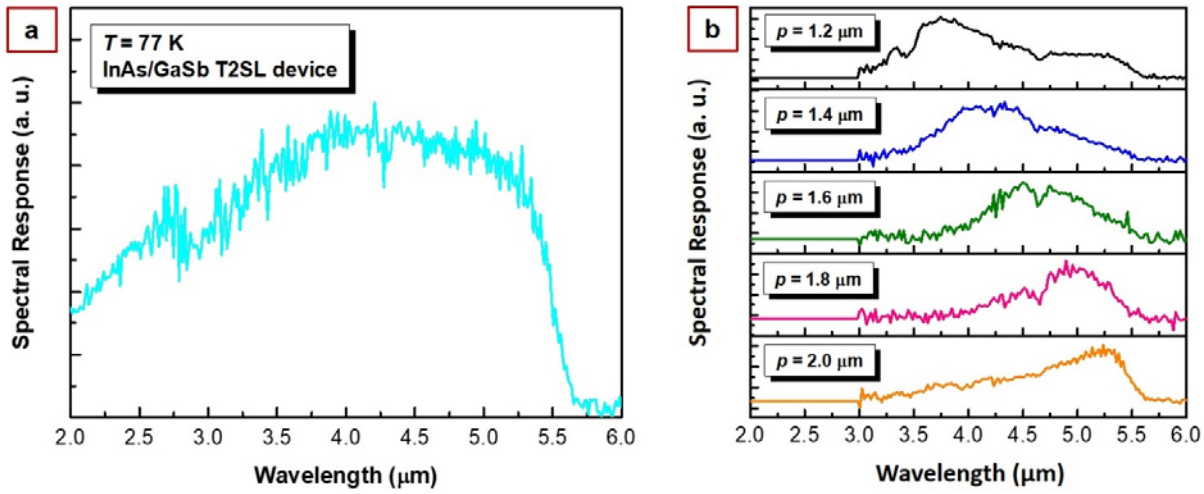

Figure 8 | Measured spectral responses at 77 K for (a) the as-fabricated T2SL photodetector and (b) the multispectral T2SL photodetector integrated with a quasi-three-dimensional coaxial aperture array with different pitches.

Fabrication of an infrared micro-polarizers integrated on a focal plane array

We interested in high performance pixelated imaging system which combine with micropolarizers and the focal plane array (FPA). To classify the objects, reflected light and emitted thermal radiation from object was used in the IR region. The polarization-based imaging techniques classify the materials by their surface roughness. Advance of nanofabrication techniques enable to make pixelated polarization imaging sensor. One of the polarizers, 1D grating offers high extinction ratio. The extinction ratio is defined as the ratio of TM-polarized light and TE-polarized light. Due to waveguide resonance between slit, transmission efficiency can be increased. We designed 2×2 superpixels of pixelated micropolarizers. Each of grating consists of subwavelength metallic gratings in four different orientations (0°, 45°, 90°, and 135°) to calculate the stoke vector. The period of each pixel is 30 μm and the metal line to prevent cross-talks is designed to have a width of 2 μm. The period (p) and width (w) of the subwavelength metallic grating are 400 nm and 200 nm, respectively.

First, an electron beam resist, ZEP 520A, was spin-coated on a silicon substrate. The grating pattern was formed using electron beam lithography. The silicon substrate was etched by $SF_6/C_4F_4/Ar$ gases, and the residual resist was etched by oxygen plasma. To prevent Si master mold from being damaged, it was coated with a hydrophobic surface by F13-TCS. The Ormostamp was dropped on the Si master mold and pressed with a PET film. The Ormostamp was cured by UV-flood exposure for 5 min with the 20 mW/cm^2 of UV-power. Then, the Ormostamp with a grating pattern was demolded from the Si mater mold. The fabrication of polarizers using UV nano-imprint lithography (UV-NIL) on sapphire was illustrated in **Figure 9**.

A 120 nm-thick of PMGI-SF3 was spin-coated as a lift-off layer and LV400 resist was spin-coated on sapphire. After hydrophobic surface modification of PET film, PET mold with pixelated polarizers was imprinted after baking LV400 and demolded after curing LV400 (Step 2). The residual of LV400 was etched by reactive ion etching (RIE) using mixture of CF_4 and O_2 gas, and the PMGI-SF3 was etched by O_2 plasma (Step 3). Finally, 10 nm of Ti and 100 nm Au were deposited onto the sample and a lift-off process was conducted with N-Methyl-2-pyrrolidone (Step 4, **Figure 10a**). As shown in **Figure 10b**, the super-pixels grating on the sapphire substrate and extended-InGaAs were integrated with an epoxy resin. After the FPA fabrication process, an InP substrate was removed by a chemical mechanical polishing (CMP) process to obtain high quantum

efficiency. Finally, the FPA and Si readout integrated circuit (ROIC) were bonded together by a flip-chip bonding process, as shown in **Figure 10c**.

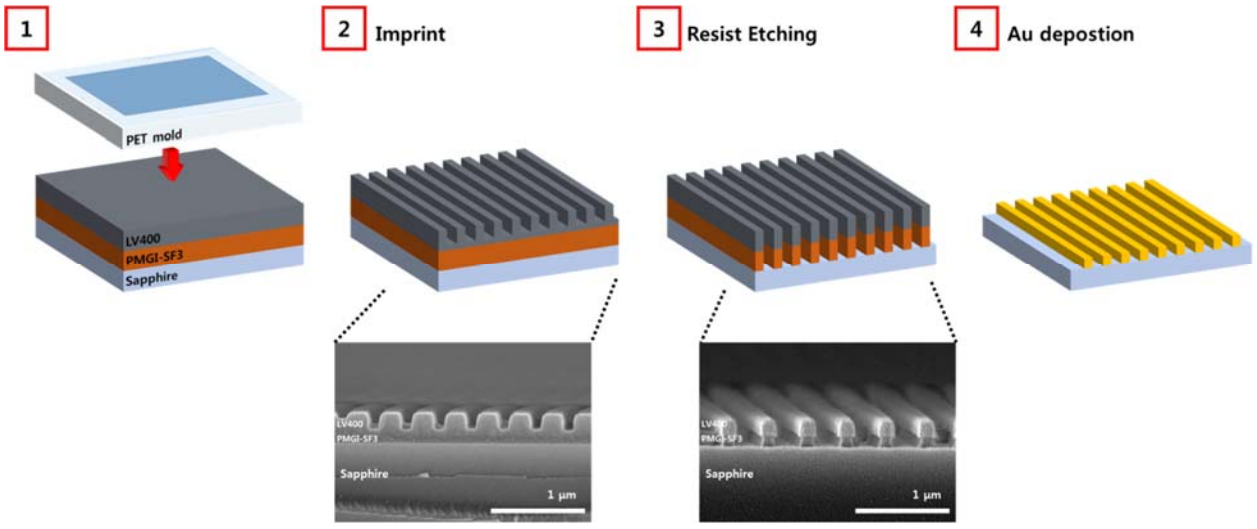

Figure 9 | Schematic of the fabrication process for the polarized 1D grating on sapphire and the measured SEM image indicating the geometrical parameters of the pitch (p) and gap width (w_{gap}).

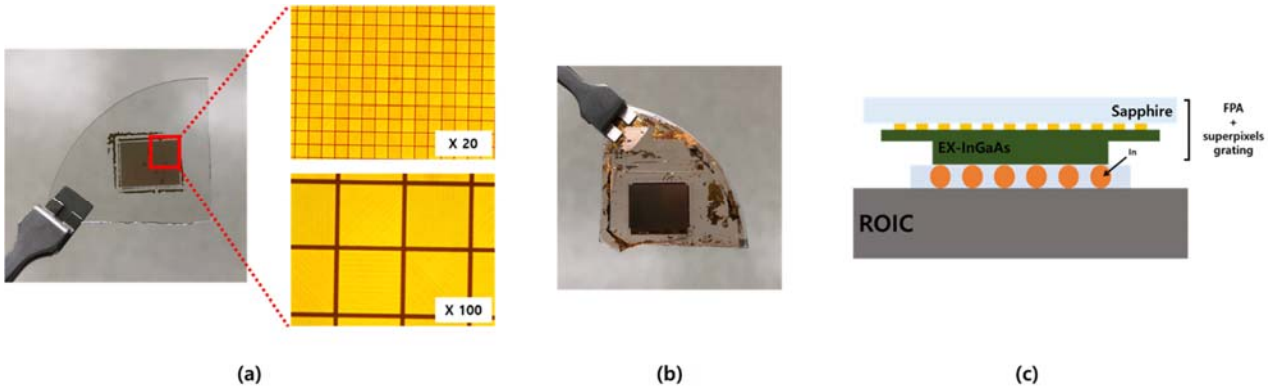

Figure 10 | Digital images of (a) 2×2 super-pixels grating on the sapphire substrate and (b) integrated extended-InGaAs epilayers on the super-pixels grating. (c) Schematic view of the super-pixels grating integrated FPA device hybridized with a Si-ROIC.